

## Subshell contributions to electron capture into the continuum in MeV/u collisions of deuterons with multielectron targets

S. Nanos <sup>1,2</sup> M. A. Quinto <sup>3</sup> I. Madesis <sup>4,2</sup> A. Laoutaris <sup>4,2</sup> T. J. M. Zouros <sup>4</sup>  
R. D. Rivarola,<sup>3,5</sup> J. M. Monti <sup>3,5</sup> and E. P. Benis <sup>1,\*</sup>

<sup>1</sup>*Department of Physics, University of Ioannina, GR-45110 Ioannina, Greece*

<sup>2</sup>*Tandem Accelerator Laboratory, INPP, NCSR “Demokritos”, GR-15310 Ag. Paraskevi, Greece*

<sup>3</sup>*Instituto de Física Rosario (CONICET-UNR), Bv 27 de Febrero 210 bis, 2000 Rosario, Argentina*

<sup>4</sup>*Department of Physics, University of Crete, GR-70013 Heraklion, Greece*

<sup>5</sup>*Laboratorio de Colisiones Atómicas, FCEIA, IFIR, Universidad Nacional de Rosario, Avenida Pellegrini 250, Rosario 2000, Argentina*



(Received 15 December 2021; accepted 25 January 2022; published 10 February 2022)

The process of the capture of a target electron into the projectile continuum (ECC) is investigated both experimentally and theoretically for collisions of 1.25–6.00 MeV deuterons with multielectron gas targets. Double-differential cross sections (DDCS),  $d^2\sigma/d\Omega dE$ , of the ECC cusp-shaped electron peak involving He, Ne, and Ar gas targets were measured at the emission angle of zero degrees with respect to the ion-beam velocity. Corresponding DDCS calculations, obtained using continuum distorted-wave (CDW) and continuum distorted-wave eikonal initial-state (CDW-EIS) theories, were critically compared to the measurements. The role of each atomic subshell of the multielectron Ne and Ar targets is examined employing the CDW-EIS theory with numerical target wave functions, which is found to best agree with the measurements.

DOI: [10.1103/PhysRevA.105.022806](https://doi.org/10.1103/PhysRevA.105.022806)

### I. INTRODUCTION

Electron emission in the interactions of fast ions with matter is a topic of continuous research interest due to its inherent application to research fields, such as astrophysical and laboratory plasmas [1,2], controlled thermonuclear fusion [3], and radiation damage of biological tissue [4], as well as due to the interest in unveiling the intricate features of the atomic structure and the underlying fundamental physical aspects. Double-differential cross-section (DDCS) electron spectra measurements have provided unique information triggering the development of advanced collision theories to describe the dynamics behind the ionization mechanisms at play, such as soft collisions, binary encounter, electron capture to the continuum, electron loss to the continuum, etc. [5]. In addition, high-resolution Auger electron spectra, superimposed on the continuum electron spectrum, have provided additional valuable state-selective information about processes such as single electron capture, transfer excitation, and transfer ionization, the detailed theoretical description of which still poses challenges to theory [6].

Particular attention has been devoted to the electron emission resulting from the capture of a target electron to the low-lying continuum states of the projectile, known as electron capture to the continuum (ECC), leading to the production of an asymmetric cusp-shaped peak at electron velocities around the projectile velocity. The combined

experimental and theoretical efforts, ever since the first unambiguous observation of the ECC cusp peak [7], attributed its formation to two-center effects due to the long-range Coulombic fields of both the projectile and the target [8]. In particular, the target field significantly influences the dynamics of the emitted electron even at large internuclear distances, as evident from the asymmetry in the low-energy wing of the cusp peak [9,10], and thus the ECC cannot be viewed in a simplified postcollision picture.

The theoretical description of the ECC process has been detailed within the framework of the continuum distorted-wave (CDW) and continuum distorted-wave eikonal initial-state (CDW-EIS) perturbative theories. Even though these theories were initially introduced to accelerate the convergence of the Born series description, during the past decades they have been used to investigate electronic collision processes such as electron capture, excitation, and ionization of atomic and molecular targets by swift bare projectiles with much success [5,11–13]. In addition, they have also been extended to describe electron emission in collisions involving dressed projectiles [14]. Different versions of these theories are obtained depending on the different approximations to the initial bound and final continuum states of the target, as well as on the action of the perturbative operator over the initial or final channel distorted-wave function (see, for example, Ref. [15]).

ECC requires a large momentum transfer to the target atom and inherently is sensitive to the shape and width of the target Compton profile. Therefore, a thorough description of the ECC process necessitates a detailed description of the target bound and continuum electronic wave functions involved in

\*mbenis@uoi.gr

the scattering process. Bare projectiles are ideal for ECC studies, as opposed to dressed projectiles for which ECC coexists with the process of electron loss to the continuum (ELC) [16,17], where projectile electrons are ionized and then captured to its continuum, resulting in a cusp-shaped peak as well. The role of the different target electron subshells in the ECC process can in principle be exposed in comparative collisions of bare ions with light targets ( $H_2$ , He) and heavier multielectron targets (Ne, Ar, etc.). Such studies have been reported in the literature for the production of the binary-encounter electron peak (BEE) [18–20].

Even though many experimental studies of electron emission include the ECC cusp peak [21–23], only a few study collisions of bare projectiles with heavy atomic targets [24]. Moreover, most studies were carried out for collision energies between 50 and 500 keV/u [25–31]. Biswas *et al.* performed a systematic study at 6 MeV/u collision energy using carbon bare ions in collisions with He and Ne targets, in an effort to compare distorted-wave (DW) theories [32] to the measurements. However, there were no measurements at zero degrees emission that expose the features of the ECC process. Considering that Coulomb ionization in the MeV collision energy range is the dominant process, ECC studies between bare ions and multielectron targets in energetic collisions provide stringent tests of the theories, exposing the dynamics of the active electron, as well as the role of the passive electrons that remain in the ionized atomic target.

Investigations of the ECC process were extended to also include neutral projectiles, antiprotons, and relativistic heavy projectiles, while imaging techniques were also implemented. Neutral He projectiles have been included in experiments studying target ionization, surprisingly showing the formation of a cusp-shaped peak due to the ECC process [33]. Antiproton impacts were considered in classical trajectory Monte Carlo calculations predicting a dip or anticusp formation at electron velocities close to the projectile velocity [10]. The ECC process had also been investigated experimentally with respect to the impact parameter using the technique of COLTRIMS [34]. Recently, ECC studies have been extended to collisions involving heavy-ion projectiles, such as uranium, and velocities in the near-relativistic regime [35]. It was shown that, for these collision conditions, the cusp peak is dominated by the process of radiative electron capture to the continuum (RECC) [36,37].

In this work, we present a systematic experimental and theoretical study of the ECC process in energetic MeV/u collisions of deuterons with He, Ne, and Ar atomic targets, in an effort to highlight the dynamic role of the atomic subshells in the ECC process. Measurements of electron DDCS at zero degrees are accompanied with theoretical results from various distorted-wave (DW) theories. Particularly, in this work we performed calculations using the *post* version of CDW (CDW-post), the *hybrid-post* version of CDW (CDW-post-hybrid), the *prior* version of CDW-EIS (CDW-EIS-prior), and a version of CDW-EIS where the initial bound and final continuum wave functions of the target are obtained numerically by a Hartree-Fock method (CDW-EIS-numerical). The theoretical calculations are critically compared to the measurements, indicating an overall better agreement for the CDW-EIS-numerical. The contribution of the atomic sub-

shells to the ECC cusp peak for the Ne and Ar targets is also presented and their role in the dynamics of the ECC process is discussed.

## II. EXPERIMENT

Cusp electron peaks were measured using the APAPES installation (Atomic Physics with Accelerators: Projectile Electron Spectroscopy) [38] operating at the NCSR “Demokritos” 5.5 MV Tandem Accelerator Laboratory [39]. The experimental setup has been described in detail elsewhere [40,41] and only a short description will be given here. The electron spectrograph consists of an electrostatic single stage hemispherical detector analyzer (HDA) equipped with a four-element injection lens and a two-dimensional position sensitive detector (2D PSD), consisting of a typical chevron type 40 mm diameter multichannel plates (MCP) detector and a resistive anode encoder (RAE). The projectile passes through the doubly differentially pumped gas cell, where it interacts with the gas target, and upon exiting the cell continues through the spectrograph to be collected in a Faraday cup for normalization purposes. The geometry of the spectrograph enables the detection of electrons emitted within a polar angle  $\theta_{max} = 0.4^\circ$  with respect to the projectile velocity. The electrons, after being focused by the spectrograph entry lens, are energetically analyzed by the HDA and imaged onto the 2D PSD within a narrow strip along the dispersion axis [42]. The setup is magnetically shielded from Earth’s magnetic field, as well as other spurious magnetic fields, by using double  $\mu$ -metal shielding.

The measured electron DDCS is determined according to the following formula [38]:

$$\text{DDCS}_j \equiv \frac{d^2\sigma_j}{d\Omega dE_j} = \frac{N_j^e}{N_l L_{\text{eff}} n \Delta\Omega \Delta E_j T \eta}, \quad (1)$$

where  $N_j^e$  is the number of electrons detected in channel  $j$  (out of 256 channels used on the PSD),  $L_{\text{eff}}$  the effective length of the target gas cell,  $N_l$  the number of ions collected in the Faraday cup,  $n$  the target gas density,  $\Delta\Omega$  the solid angle determined by the entry aperture of the lens and the distance of the center of the target gas cell from it,  $\Delta E_j$  the energy step per channel in the spectrum, and  $T$  the analyzer transmission determined by three electroformed meshes of 90% transmission each. The overall efficiency,  $\eta$ , was determined from measurements of the BEE peak for the 1.50 MeV  $d + \text{He}$  collision system. The resulting BEE electron yield, as determined from Eq. (1) except for the overall efficiency  $\eta$ , was normalized to the corresponding theoretical BEE DDCS calculated within a DW theory, as commonly done in zero-degree projectile spectroscopy [38]. For this purpose, the calculations of the CDW-EIS-numerical theory were preferred, as it better fit to the BEE peak, resulting in an overall detection efficiency of  $\eta = (50 \pm 5)\%$ . The measured electron DDCS spectra covering the area between the low-energy wing of the cusp peak and the high-energy wing of the BEE peak are shown in Fig. 1, along with the corresponding DDCS calculations from the four DW theories examined in this work. It should be noted that the electron energy where the maximum of the cusp peak occurs coincides with the reduced projectile energy  $t_p$

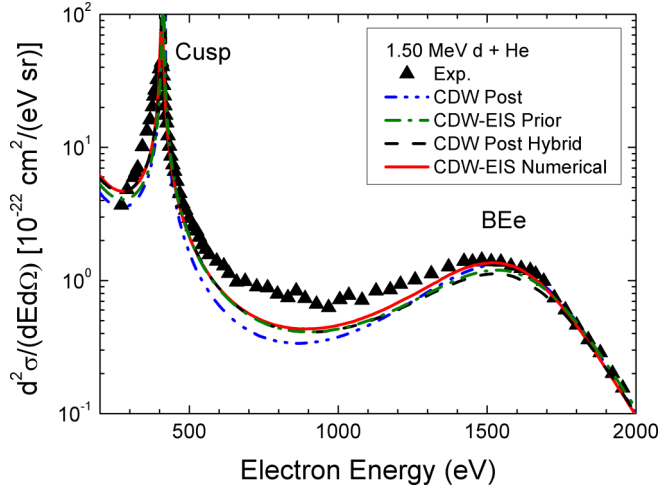


FIG. 1. DDCS electron spectra measured at zero degrees with respect to the projectile velocity for collisions of 1.50 MeV deuterons with He gas targets. Symbols: experimental data. Lines: DW theories' calculations (see text). The spectral locations of the cusp and BEE peaks are depicted.

determined as [38]

$$t_p = \frac{m}{M_p} E_p = 548.58 \frac{E_p(\text{MeV})}{M_p(\text{amu})} (\text{eV}), \quad (2)$$

where  $E_p$  and  $M_p$  are the kinetic energy and mass of the projectile, respectively, while  $m$  is the electron mass.

The APAPES setup has been primarily developed for zero-degree Auger projectile electron spectroscopy (ZAPS) studies [41] since zero-degree observation offers the best Auger projectile electron energy resolution. The use of 2D PSD and preretardation entry lens within the overall spectrograph allows for performing high-resolution and high efficiency measurements. Here, we extended the use of the spectrograph to perform low-resolution measurements of cusp electrons. It should be noted that a typical ZAPS spectrum can be recorded simultaneously in one energy window covering an energy range of about 20% of the tuning electron energy. However, this energy range is not wide enough to cover the spectral area of the entire cusp peak. Thus several overlapped energy windows, obtained at the appropriate tuning energies, were pieced together as necessary. An example of such piecing together of four overlapping energy windows, corresponding to the tuning energies of  $W = 585, 685, 800,$  and  $940$  eV, is shown in Fig. 2 (multicolored opened circles) for the collision system  $1.50 \text{ MeV } p + \text{He}$ .

For each spectrum a subtraction of the background signal, corresponding to a measurement without target gas, was performed. The resulting spectrum was energy calibrated according to known energy vs channel calibration formulas, and the DDCS were then obtained according to Eq. (1). Single collision conditions were ensured by properly adjusting the target gas pressure. Due to the large number of detection channels in each energy window we performed a weighted averaging of the data to improve the visibility of the cusp peak. In Fig. 2, the statistical uncertainty of the averaged data is within the size of the symbol, while no statistical error bars are shown in the four overlapping energy windows

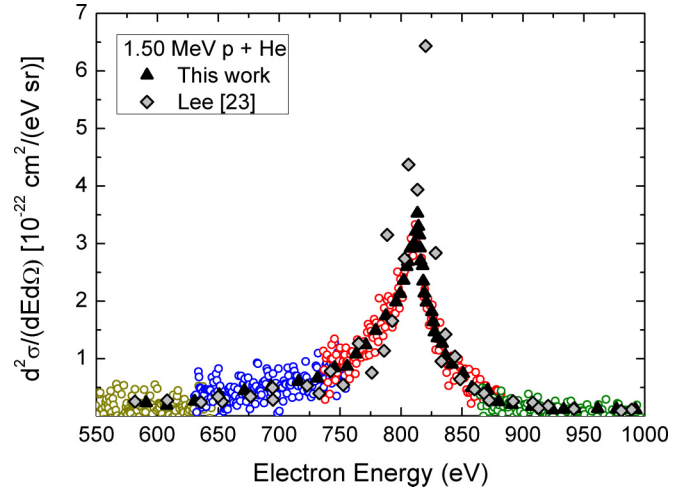


FIG. 2. DDCS electron spectra measured at zero degrees with respect to the projectile velocity for collisions of 1.50 MeV protons with He gas targets. Triangles: experimental data obtained in this work. Diamonds: experimental data retrieved from [23]. Multicolored circles: the four overlapping energy windows covering the ECC cusp peak, the weighted average of which corresponds to the triangles.

for presentation purposes. An overall absolute uncertainty of about 15% is inherent in all our measurements. The thus obtained DDCS spectra are then compared to older measurements reported in [23], showing an excellent agreement. Note that the data in [23] were taken with a tandem parallel-plate spectrometer having a smaller solid angle as compared to our spectrograph, which justifies larger DDCS values at the cusp peak maximum. Accordingly, in Fig. 1 the measured spectrum is obtained after piecing together 13 overlapping energy windows. Deuterons were preferred over protons for most cases in this work in order to maintain the electron energies below the value of 3 keV, close to the upper limit currently allowed by our spectrograph.

### III. THEORY

#### A. CDW theory

The CDW distorted-wave theory was initially developed to study single electron capture, and later single electron ionization, from mono-electronic targets by bare projectile impact [43–45]. The extension to multi-electronic targets can be made following the work by Fainstein *et al.* [46] (see also [5,8] and references therein) where it is shown that, for single ionization from bare-ion impact, within the independent electron model, a multi-electronic system can be reduced to a mono-electronic one. Within the independent electron model, and considering one active electron (the one to be ionized), the target potential  $V_T$  can be written as

$$V_T(\mathbf{x}) = -\frac{Z_T}{x} + V_{ap}(\mathbf{x}), \quad (3)$$

where  $\mathbf{x}$  is the active electron coordinate in the target reference frame. The first term describes the Coulomb interaction between the active-electron and the target nuclear charge  $Z_T$ , whereas the second one involves the electrostatic interaction

between the active electron and the passive ones, which are assumed to remain frozen in their initial subshells throughout the collision process [47].

The CDW approximation is the first order of a distorted-wave series in which the initial and final distorted waves are proposed as

$$\chi_i^+(\mathbf{x}, t) = \Phi_i(\mathbf{x}, t) \mathcal{L}_i^+(s) \quad (4)$$

$$= \phi_i(\mathbf{x}) \exp(-i \varepsilon_i t) \mathcal{L}_i^+(s) \quad (5)$$

and

$$\chi_f^-(\mathbf{x}, t) = \Phi_f(\mathbf{x}, t) \mathcal{L}_f^-(s) \quad (6)$$

$$= \phi_f(\mathbf{x}) \exp(-i \varepsilon_f t) \mathcal{L}_f^-(s), \quad (7)$$

respectively, with  $s$  being the active electron coordinate in projectile reference frame. In Eq. (4) and in Eq. (6),  $\Phi_i(\mathbf{x}, t)$  and  $\Phi_f(\mathbf{x}, t)$  are the initial bound and final continuum state solutions of the time-dependent target Schrödinger equation. In Eq. (5),  $\varepsilon_i$  is the electron energy in the initial bound state, whereas, in Eq. (7),  $\varepsilon_f = \frac{1}{2}k^2$  is the electron energy in the final state,  $\mathbf{k}$  being the linear momentum of the ejected electron in the target reference frame.

The initial distortion is proposed as

$$\mathcal{L}_i^+(s) = N(v) {}_1F_1[i\nu; 1; i(vs + \mathbf{v} \cdot s)], \quad (8)$$

whereas the final distortion is chosen as

$$\mathcal{L}_f^-(s) = N^*(\zeta) {}_1F_1[-i\zeta; 1; -i(ps + \mathbf{p} \cdot s)], \quad (9)$$

where  $\mathbf{v}$  is the projectile velocity,  $v = Z_p/v$ ,  $\zeta = Z_p/p$ ,  $\mathbf{p} = \mathbf{k} - \mathbf{v}$  is the ejected electron momentum in the projectile reference frame, and  $N(a) = \exp(\pi a/2)\Gamma(1 + ia)$  (with  $\Gamma$  being the Euler Gamma function) is the normalization factor of the  ${}_1F_1$  hypergeometric function.

The initial bound state of the target  $\phi_i$  and its binding energy  $\varepsilon_i$  in Eq. (5) is calculated by means of RHF wave functions (see [48] and the Appendix from [49]). On the other hand, the target final continuum state  $\phi_f$  is chosen as an analytical hydrogenlike continuum function:

$$\phi_f(\mathbf{x}) = \frac{1}{(2\pi)^{3/2}} \exp(i\mathbf{k} \cdot \mathbf{x}) \times N^*(\lambda) {}_1F_1[-i\lambda; 1, -i(kx + \mathbf{k} \cdot \mathbf{x})], \quad (10)$$

with  $\lambda = \tilde{Z}_T/k$ , where  $\tilde{Z}_T$  is an effective or net target charge to be chosen. This approximation has been previously used with success for electron capture [45]. It implies the replacement of the target potential by effective Coulombic ones for each target orbital in the final channel. However, this implies the loss of orthogonalization between initial and final states.

Finally, the double-differential cross section in electron emission energy ( $E_k$ ) and solid ejection angles is obtained as [47]

$$\frac{d^2\sigma^\pm}{dE_k d\Omega_k} = k \int d\boldsymbol{\eta} |\mathcal{R}_{if}^\pm(\boldsymbol{\eta})|^2, \quad (11)$$

with  $\mathcal{R}_{if}^\pm(\boldsymbol{\eta})$  being the scattering matrix element as a function of the transverse momentum transfer  $\boldsymbol{\eta}$ , with the  $-$  ( $+$ ) sign denoting its *prior* (*post*) form. The transition amplitude obtained with the *prior* version of the CDW theory is known to have intrinsic divergences that forbid its correct integration to

TABLE I. Parameters  $d$  (a.u.) and  $K$  (a.u.) of the GSZ potential for the different targets considered, extracted from [50].

Target	$d$	$K$
He	0.381	1.77
Ne	0.558	2.71
Ar	1.045	3.50

obtain the differential cross sections [15]. Therefore, we shall work with the *post* CDW one.

The *post* CDW operator  $W^{\text{CDW-}}$  is given by

$$W_f^{\text{CDW-}} \chi_f^- = \Phi_f(\mathbf{x}, t) [\nabla_{\mathbf{x}} \ln \phi_f(\mathbf{x}) \cdot \nabla_s \mathcal{L}_f^-(s)] + \tilde{V}_T(\mathbf{x}) \chi_f^-, \quad (12)$$

where the first term is the well known *post* CDW perturbative operator and the second one is related to an additional potential left unsolved by the choice of  $\phi_f$ ,

$$\tilde{V}_T(\mathbf{x}) = -(Z_T - \tilde{Z}_T)/x + V_{ap}(\mathbf{x}), \quad (13)$$

with  $V_{ap}(\mathbf{x})$  being the interaction between the active electron and the passive ones [47]. This  $\tilde{V}_T$  potential is excluded in the usual *post* version of the CDW theory. We choose  $\tilde{Z}_T = n_i \sqrt{-2\varepsilon_i}$  (see [45]), with  $n_i$  the principal quantum number of the initial bound subshell, as the effective charge describing the hydrogenlike continuum for the residual target continuum final state. However, in order to take into account the non-Coulombic part of the interaction between the active and passive electrons the  $\tilde{V}_T$  potential is included in a more complete CDW approximation.

Following the work of [49] we consider  $\tilde{V}_T$  in terms of a GSZ analytical parametric potential [50], and rewrite Eq. (13), giving

$$\tilde{V}_T(\mathbf{x}) = -\frac{(q - \tilde{Z}_T)}{x} - \frac{(Z_T - q)}{x} \Omega(x), \quad (14)$$

with

$$\Omega(x) = [H(e^{x/d} - 1) + 1]^{-1}, \quad (15)$$

$q = Z_T - N$  being the net charge of the target, with  $N$  the number of passive electrons, and  $d$  and  $H(= d \times K)$  parameters dependent on  $Z_T$  and  $N$  (see [50], and references therein). The parameters used for each target are shown in Table I.

The transition amplitude for the *post* version of CDW is

$$\mathcal{R}_{if}^+(\boldsymbol{\eta}) = -i \frac{4\pi^2}{v} \mathbf{F}^{a+}(\mathbf{K}) \cdot \mathbf{G}^{a+}(\mathbf{K}), \quad (16)$$

where  $\mathbf{K}$  is the momentum transfer in the center of mass of the system. Explicit expressions of  $\mathbf{F}^{a+}$  and  $\mathbf{G}^{a+}$  can be found in [15].

In order to include the dynamic screening in the *post* version of CDW and to avoid the intrinsic divergences found in it, a *complete hybrid* version is proposed (see [15]):

$$\mathcal{R}_{if}^+(\boldsymbol{\eta}) = -i \frac{4\pi^2}{v} [\mathbf{F}^{a+}(\mathbf{K}) \cdot \mathbf{G}^{a+}(\mathbf{K}) + F^{b+}(\mathbf{K}) G^{b+}(\mathbf{K})]. \quad (17)$$

Explicit expressions of  $\mathbf{F}^{a+}$ ,  $F^{b+}$ ,  $\mathbf{G}^{a+}$ , and  $G^{b+}$  can be found in [15]. In  $G^{b+}$  of Eq. (17),  $\mathcal{L}_i^+$  is considered as an eikonal

phase given by

$$\lim_{vs \rightarrow \infty} \mathcal{L}_i^+(s) \equiv \mathcal{L}_i^{\text{EIS}+}(s) = \exp[-i v \ln(vs + v \cdot s)]. \quad (18)$$

### B. CDW-EIS theory

The CDW-EIS theory was first introduced by Crothers and McCaan [51] to solve the lack of normalization of the initial channel projectile distortion when studying electron ionization by bare ions. In this theory the initial channel projectile distortion is proposed as

$$\mathcal{L}_i^{\text{EIS}+}(s) = \exp[-i v \ln(vs + v \cdot s)]. \quad (19)$$

The final channel projectile distortion is considered as in Eq. (9).

The *prior* version of the CDW-EIS approximation is free of any divergences and the perturbative operator  $W^{\text{EIS}+}$  results as

$$W_i^{\text{EIS}+} \chi_i^+ = \Phi_i(\mathbf{x}, t) \left[ \frac{1}{2} \nabla_s^2 \mathcal{L}_i^+(s) + \nabla_x \ln \phi_i(\mathbf{x}) \cdot \nabla_s \mathcal{L}_i^+(s) \right]. \quad (20)$$

The initial bound and final continuum target wave functions are considered as in the above-mentioned CDW theory. Explicit expression for the *prior* CDW-EIS transition amplitude can be found elsewhere [47].

Instead of approximating the final target continuum by an effective Coulomb one, the initial bound and final continuum target wave functions can be obtained by numerically solving the target Schrödinger equation. The procedure to obtain the transition amplitude within this theory was shown by Gulyás *et al.* [52], thus resulting in the *numerical* version of the CDW-EIS theory. By doing so, the orthogonality between the initial bound and final continuum target wave functions is maintained. It is worth mentioning that, when calculating the initial bound states in this *numerical* version of CDW-EIS, the binding energies,  $\varepsilon_i$ , considered for each subshell were those provided by Clementi and Roetti [48].

## IV. RESULTS AND DISCUSSION

In this section, we present a comparative study between the calculations of the DW theories for the ECC cusp peak and the corresponding electron DDCS measured at zero degrees emission angle with respect to the projectile velocity, for energetic collisions of deuterons with multielectron Ne and Ar gas targets. Ion-atom collision processes are inherently of a many-body nature that usually necessitates the modeling of the passive target and projectile electrons. In this context, He atoms can be considered as a benchmark target for the collision models since their two electrons in the ground state are easier to describe as compared to higher atomic number multielectron targets. In order to benefit our comparative study from such benchmark calculations, we have also measured the electron DDCS for the collision system of 1.50 MeV deuterons with He gas targets, covering the energy range from the cusp peak up to the BEE peak, as mentioned earlier. In Fig. 1 we present the experimental DDCS electron spectra along with the results from the DW theories examined in this work.

An overall similar behavior with small, but substantial differences for all the DW theories is evident from Fig. 1, with all

theories converging at the high-energy wing of the BEE peak. Small variations start to arise at the maximum of the BEE peak. Based on the absolute normalization of our measured electron yield to the BEE peak obtained from DW calculations, as mentioned earlier, it is seen that CDW-EIS-numerical calculations better fit to the measurements. Similarly, although all the calculations of the DW theories are seen to be in close agreement at the high-energy wing of the ECC cusp peak, they show substantial differences at the low-energy ECC cusp peak wing. It should be mentioned here that a recently developed four-body CDW-EIS theory seems to be in better agreement with similar DDCS measurements involving collisions of protons with He targets [53], but it is not included here as it is valid for two-electron targets only. Moreover, our theoretical zero-degree DDCS calculations were not averaged over the experimental polar angle  $\theta$ , as this would have mostly affected the DDCS height of the cusp peak at the pole area, leaving the cusp wings essentially unaffected. For the same reason we did not convolute the DDCS calculations with the experimental resolution ( $\Delta E/E \simeq 1\%$ ), since the latter is of the order of the energy step of the calculations. For the electrons in the valley between the cusp and BEE peaks, all DW theories seem to underestimate the experimental DDCS.

In Fig. 3, we present our experimental DDCS, along with the corresponding DDCS from the DW theories, obtained in collisions of deuterons with Ne and Ar targets at the collision energies of 1.50, 3.00, and 6.00 MeV. The experiments were performed under the same conditions for each target, except for the value of the gas pressure that was determined according to the single collision conditions (typically 5 to 20 mTorr). Four overlapping energy windows were pieced together to adequately cover the cusp peak at the 1.50 and 3.00 MeV collision energies, while three energy windows were used for the corresponding 6.00 MeV collision energy.

For the case of the Ne target at 1.50 MeV collision energy, CDW-post results are seen to differ the most from the results of the other theories, showing the lowest DDCS value in lesser agreement with the data. The results from the other DW theories are seen to slightly overestimate the high-energy wing of the ECC cusp peak in very close agreement with each other. However, at the low-energy wing of the ECC peak, CDW-EIS-numerical is seen to be in better agreement with the measurements, while the CDW-EIS-prior and CDW-post-hybrid are close to each other, but showing lower DDCS values. This behavior of the four considered theories is qualitatively maintained as the collision energy increases.

For the case of the Ar target, the behavior is different to a certain extent compared to Ne target. At 1.50 MeV collision energy, all the theories considered are seen to produce very similar results, all in good agreement with the low-energy wing of the ECC cusp peak, but with an overestimation of the DDCS in the high-energy wing. However, for the higher collision energies, at 3.00 MeV and more pronounced at 6.00 MeV, the present theoretical results follow the qualitative behavior described for the Ne target. These effects are attributed to the contributions of the different atomic subshells to the ECC process depending on the collision energy and will be detailed below.

We should note that in a previous paper the influence of the representation of the initial bound state was shown to play an

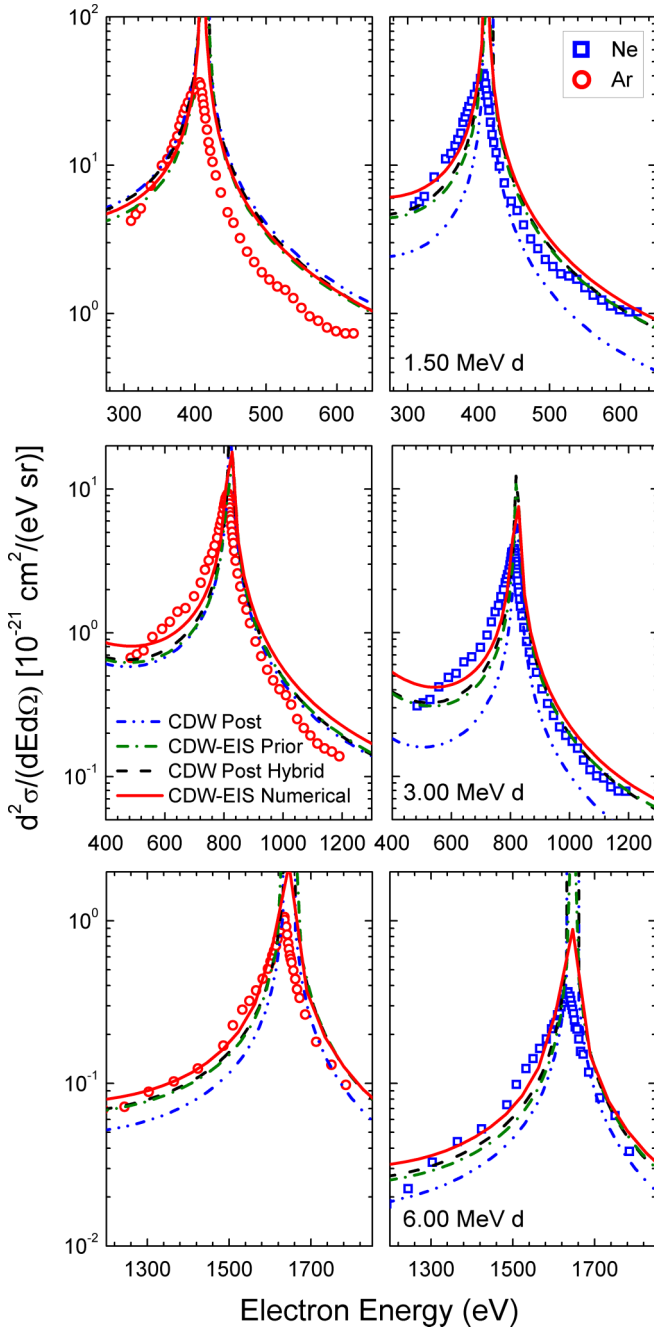


FIG. 3. Electron DDCS measured at zero degrees with respect to the projectile velocity for collisions of [top] 1.50 MeV, [middle] 3.00 MeV, and [bottom] 6.00 MeV deuterons with [right] Ne and [left] Ar gas targets. The symbols correspond to the experimental data and the lines to the calculations of (blue dash-dot-dotted line) CDW-post, (green dash-dotted line) CDW-EIS-prior, (black dashed line) CDW-post-hybrid, and (red line) CDW-EIS-numerical.

important role in the description of electron emission spectra. In [54] an optimized potential model was employed instead of a Hartree-Fock-Slater one, to calculate the initial state. It could be interesting to investigate how this initial bound-state representation affects the asymmetry and height of the ECC cusp.

In an effort to go deeper into these effects and their causes, we examined in more detail the collision energies in

the range of 1.25 to 2.00 MeV. Earlier studies using proton beams have reported single differential cross-section ECC measurements (SDCS,  $d\sigma/d\Omega$ ) showing a crossing of the Ne and Ar SDCS as a function of the collision energy in the area between 0.625 and 1.00 MeV [24] that corresponds to the range of collision energies of 1.25 to 2.00 MeV for deuterons. Thus we focused our study in this collision energy region, providing a stringent test for the DW theories under examination.

In Fig. 4 (top), we present our experimental DDCS for the collision system of deuterons with Ne and Ar targets for the collision energies of 1.25, 1.50, 1.75, and 2.00 MeV. It is clearly seen that, while the DDCS for Ne are larger than for Ar at the collision energy of 1.25 MeV, they become smaller at the collision energy of 2.00 MeV. A subtle change in the magnitude of the DDCS for Ne and Ar is evident between the collision energies of 1.50 and 1.75 MeV, in agreement with the corresponding SDCS results reported in [24]. This feature, exposed here in the DDCS level of detail, is unambiguously attributed to the contribution of the atomic subshells of the targets to the ionization process. Our theoretical results show that only the CDW-EIS-numerical theory can reliably reproduce this experimental result, whilst the other three considered CDW theories qualitatively reproduce the effect to some degree, but only at lower collision energies. In Fig. 4 (bottom), we present our DDCS calculations for the CDW-EIS-numerical theory in comparison to the corresponding measurements.

The success of the CDW-EIS-numerical theory in reproducing the change in the magnitude of the DDCS for Ne and Ar calls for a deeper investigation of the contribution of the different atomic subshells to the ionization process. In Fig. 5, we present CDW-EIS-numerical calculations about the contributions of the Ne and Ar atomic subshells to the formation of the ECC cusp peak in collisions with 1.25, 1.50, 1.75, 2.00, 3.00, and 6.00 MeV deuterons. The contribution of different magnetic quantum numbers of  $nl$  subshells are considered in the theoretical calculations by averaging over them. In general, one may argue that the relative contribution of each subshell to the ECC peak is largely governed by the relation between the electron linear velocity in that given initial subshell and the projectile velocity, the subshell binding energy, and the number of electrons in a given subshell. Details on subshell binding energies and velocities, as well as the projectile energies and velocities, are given in Table II. However, such relations may serve only as a rough guide and cannot be used for finer predictions. From Fig. 5 (top), it is seen that, for the Ne case, the  $2p$  and  $2s$  subshells' contributions decrease with increasing the collision energy, with a faster decrease for the  $2p$  subshell. The one order of magnitude difference at the collision energy of 1.25 MeV has essentially vanished at the collision energy of 6.00 MeV. On the other hand, the contribution of the  $1s$  subshell increases with increasing collision energy resulting in a larger contribution than the  $2s$  and  $2p$  subshells at the collision energy of 6.00 MeV. In the latter case, the velocity of the ion beam is much closer to the linear velocity of the  $1s$  subshell than the  $2s$  and  $2p$  subshells (see Table II), partially justifying such a behavior. However, the most important observation for the Ne case is that, in the collision energy range of 1.25 to 2.00 MeV,

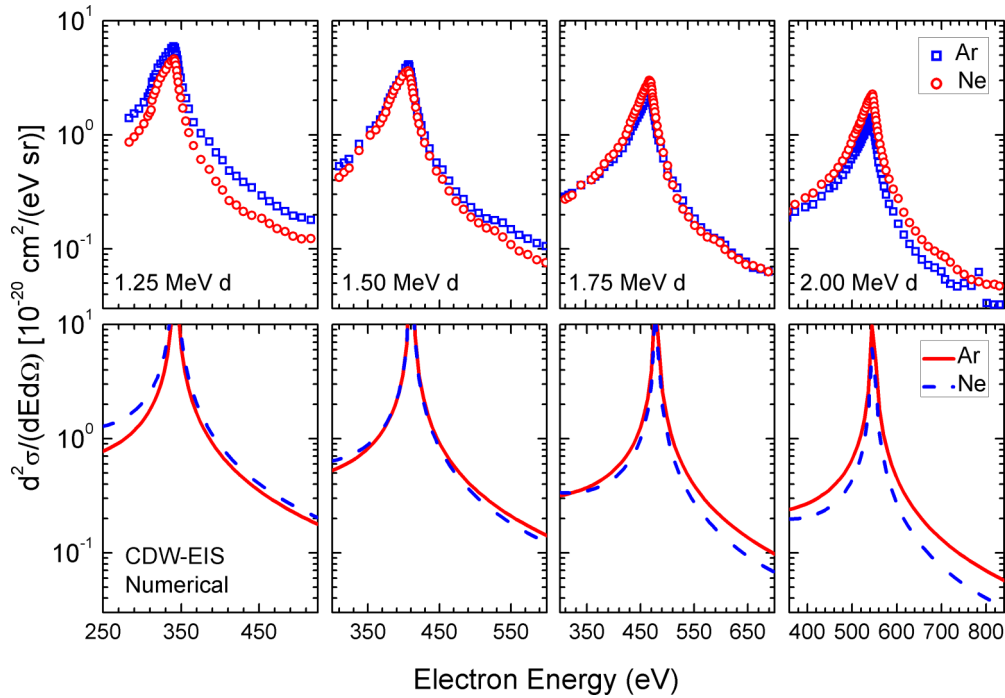


FIG. 4. Electron DDCS measured at zero degrees with respect to the projectile velocity for collisions of 1.25–2.00 MeV deuterons with Ar (red) and Ne (blue) gas targets. The symbols correspond to the measurements and the lines to the calculations of the CDW-EIS-numerical theory. The small peak around 800 eV in the Ne spectrum of 2.00 MeV collision energy corresponds to the Ne-KLL Auger lines.

the largest contribution to the EEC cusp peak comes from the  $2p$  subshell.

From Fig. 5 (bottom), it is seen that, for the Ar case, the  $3p$  and  $3s$  subshells' contribution decreases with increasing collision energy, with a faster decrease for the  $3s$  subshell.

This could be due to the higher binding energy of the  $3s$  subshell compared to the  $3p$  subshell (see Table II), as both subshells have quite similar linear velocities. Interestingly, the  $2p$  and  $2s$  contributions seem to be quite insensitive to the dependence of the collision energy for the energy range of

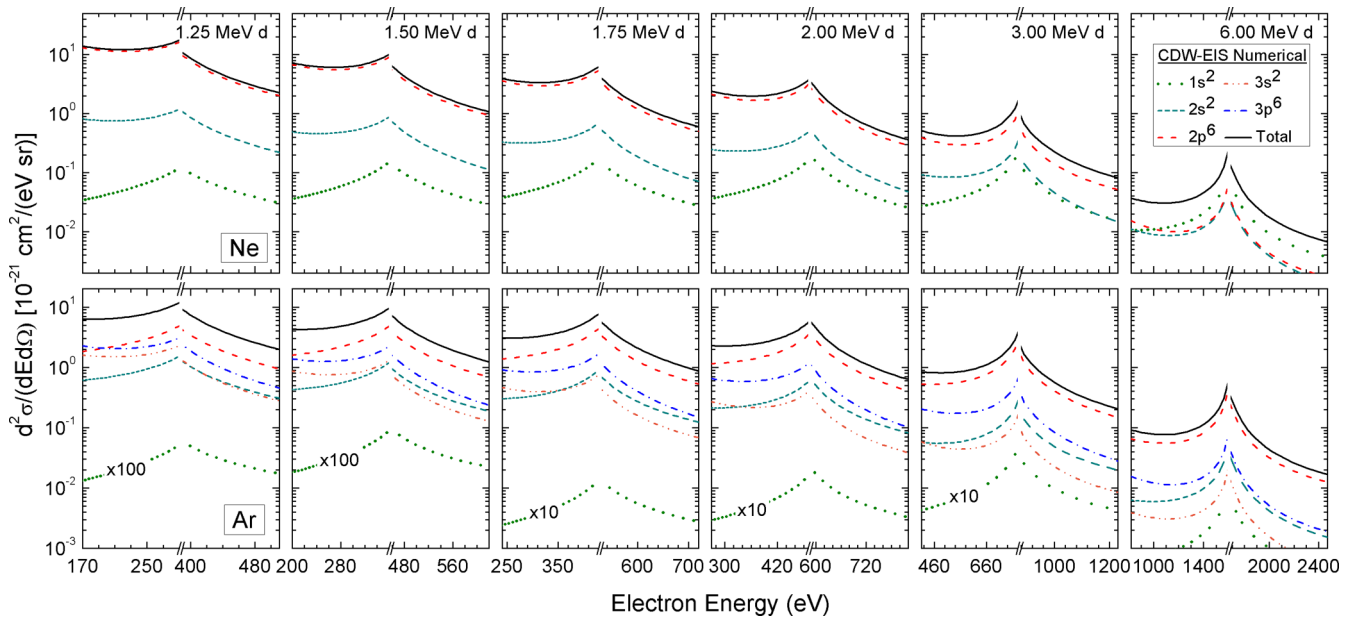


FIG. 5. Contributions of the Ne [top] and Ar [bottom] atomic subshells to the formation of the ECC cusp peak in collisions with (from left to right) 1.25, 1.50, 1.75, 2.00, 3.00, and 6.00 MeV deuterons, corresponding to the CDW-EIS-numerical calculations. The break in the electron energy axes around the region of the pole of the cusp peak is to facilitate visibility. Note that the  $1s$  contribution for Ar is multiplied by the factor of 100 for the collision energies of 1.25 and 1.50 MeV and by the factor of 10 for the collision energies of 1.75, 2.00, and 3.00 MeV, respectively.

TABLE II. Subshell linear velocities,  $v_i$  (a.u.) [55], and binding energies,  $\varepsilon_i$  (a.u.) [48], for the Ne and Ar atoms, and deuteron projectile velocities,  $v$  (a.u.), for the different collision energies  $E_p$  (MeV) considered in Fig. 5.

Ne	1s	2s	2p			
$ \varepsilon_i $	32.772	1.930	0.850			
$v_i$	8.113	1.299	2.500			
Ar	1s	2s	2p	3s	3p	
$ \varepsilon_i $	118.610	12.322	9.572	1.277	0.591	
$v_i$	14.832	4.574	6.138	1.535	1.663	
$E_p$	1.25	1.50	1.75	2.00	3.00	6.00
$v$	7.074	7.749	8.370	8.948	10.959	15.498

1.25 to 2.00 MeV, showing only a very small decrease. The contribution reduction becomes visible at the 3.00 MeV and much more visible at the 6.00 MeV collision energies. The contribution of the 1s subshell is negligible and only at the highest collision energy of 6.00 MeV becomes noticeable. As in the case of Ne, the contribution of the 1s subshell is increasing with increasing collision energy, as would be expected from velocity matching arguments. In the case of Ar, the most important observation is that, in the collision energy range of 1.25 to 2.00 MeV, the largest contribution to the ECC cusp peak comes from the 2p subshell for which an almost constant cross section is predicted by the CDW-EIS-numerical theory. This delicate difference between the 2p contributions for the Ne and Ar cases seems to account for their DDCS crossing presented in Fig. 4.

An analysis similar to the one presented in Fig. 5 was performed for the other DW theories considered here as well. A similar behavior for the general trends of the subshell contributions was observed, but with essential differences in their detailed behavior resulting in less accurate predictions as compared to the CDW-EIS-numerical calculations, for the range of collision energies considered in this work. To further investigate the source of the DDCS differences between the DW theories we compared the initial radial wave functions between the Clementi-Roetti wave function used in CDW-EIS-prior and the HF-numerical used in CDW-EIS-numerical. Their comparison showed minor differences, not likely to account for the difference in DDCS. This is a strong indication that the differences between CDW-EIS-prior and CDW-EIS-numerical can be attributed to the final continuum function.

## V. CONCLUSIONS

We have presented experimental and theoretical DDCS for the ECC cusp-shaped electron peak formed in collisions of

1.25–6.00 MeV deuterons with He, Ne, and Ar targets. The cusp electrons were measured at zero degrees with respect to the ion-beam velocity, while the corresponding calculations were performed within four DW theories, namely the *post* and *hybrid-post* versions of CDW, the *prior* version of CDW-EIS, and the CDW-EIS-numerical, a version of CDW-EIS where the initial bound and final continuum wave functions of the target are obtained numerically by a Hartree-Fock method. The cusp DDCS calculations of the DW theories are critically compared to the measurements, indicating an overall better agreement for the CDW-EIS-numerical. The differences in the results of the DW theories are attributed primarily to the contributions of the different atomic subshells to the ECC process. The role of each atomic subshell of the multielectron Ne and Ar targets, regarding its contribution to the ECC cusp peak, has been calculated for all the experimental collision energies using the CDW-EIS-numerical theory. The calculations showed that for both atomic targets the main contribution to the ECC cusp peak comes from the 2p subshell for the collision energy region of 1.25 to 3.00 MeV. Interestingly, for the collision energy region of 1.25 to 2.00 MeV, the 2p subshell contribution seems to remain almost constant for Ar, while for Ne it substantially decreases with increasing collision energy. This behavior seems to account for the subtle change in the magnitude of the DDCS for Ne and Ar observed experimentally in the above region of collision energies, that only the CDW-EIS-numerical theory reproduced reliably.

The critical comparison of the DW theories to the ECC cusp DDCS measurements and the success of the CDW-EIS-numerical theory should be regarded as a first step towards future studies that will include different conditions (e.g., dressed projectiles) and wider electron energy regions (e.g., soft electrons) in order to safer assess the validity and applicability of the various approximations.

## ACKNOWLEDGMENTS

S.N., I.M., A.L., T.J.M.Z., and E.P.B. acknowledge support by the project “Cluster of Accelerator Laboratories for Ion-Beam Research and Applications–CALIBRA” (No. MIS 5002799), which is implemented under the Action “Reinforcement of the Research and Innovation Infrastructure,” funded by the Operational Programme “Competitiveness, Entrepreneurship and Innovation” (NSRF 2014-2020) and cofinanced by Greece and the European Union (European Regional Development Fund). J.M.M., R.D.R., and M.A.Q. acknowledge financial support from Consejo Nacional de Investigaciones Científicas y Técnicas of Argentina.

- [1] P. Beiersdorfer, Laboratory X-ray astrophysics, *Annu. Rev. Astron. Astrophys.* **41**, 343 (2003).
- [2] H. Takabe and Y. Kuramitsu, Recent progress of laboratory astrophysics with intense lasers, *High Power Laser Sci. Eng.* **9**, e49 (2021).
- [3] R. Betti and O. A. Hurricane, Inertial-confinement fusion with lasers, *Nat. Phys.* **12**, 435 (2016).

- [4] G. Tsakanova, N. Babayan, E. Karalova, L. Hakobyan, L. Abroyan, A. Avetisyan, H. Avagyan, S. Hakobyan, A. Poghosyan, B. Baghdasaryan, E. Arakelova, V. Ayvazyan, L. Matevosyan, A. Navasardyan, H. Davtyan, L. Apresyan, A. Yeremyan, R. Aroutiounian, A. N. Osipov, B. Grigoryan *et al.*, Low-energy laser-driven ultrashort pulsed electron beam irradiation-induced immune response in rats, *Int. J. Mol. Sci.* **22**, 11525 (2021).

- [5] N. Stolterfoht, R. DuBois, and R. Rivarola, *Electron Emission in Heavy Ion-Atom Collisions*, Springer Series on Atomic, Optical, and Plasma Physics (Springer-Verlag, Berlin, 1997).
- [6] I. Madesis, A. Laoutaris, T. J. M. Zouros, E. P. Benis, J. W. Gao, and A. Dubois, Pauli Shielding and Breakdown of Spin Statistics in Multielectron Multi-Open-Shell Dynamical Atomic Systems, *Phys. Rev. Lett.* **124**, 113401 (2020).
- [7] G. B. Crooks and M. E. Rudd, Experimental Evidence for the Mechanism of Charge Transfer into Continuum States, *Phys. Rev. Lett.* **25**, 1599 (1970).
- [8] P. D. Fainstein, V. H. Ponce, and R. D. Rivarola, Two-centre effects in ionization by ion impact, *J. Phys. B: At., Mol. Phys.* **24**, 3091 (1991).
- [9] G. C. Bernardi, S. Suárez, P. D. Fainstein, C. R. Garibotti, W. Meckbach, and P. Focke, Two-center effects in electron emission in  ${}^3\text{He}^{2+}$ -He and  $\text{H}^+$ -He collisions at intermediate energies, *Phys. Rev. A* **40**, 6863 (1989).
- [10] C. O. Reinhold and D. R. Schultz, Anticusp and binary peak structures in the electronic spectra arising from proton- and antiproton-helium collisions, *Phys. Rev. A* **40**, 7373 (1989).
- [11] P. N. Abufager, A. E. Martínez, R. D. Rivarola, and P. D. Fainstein, CDW-EIS model for single-electron capture in ion-atom collisions involving multielectronic targets, *J. Phys. B: At., Mol. Phys.* **37**, 817 (2004).
- [12] M. A. Quinto, P. R. Montenegro, J. M. Monti, O. A. Fojón, and R. D. Rivarola, Electron capture by swift ions from molecules of biological interest, *J. Phys. B: At., Mol. Phys.* **51**, 165201 (2018).
- [13] C. A. Ramirez and R. D. Rivarola, Electron excitation of hydrogenic targets in collisions with ions or atoms, *J. Phys. B: At., Mol. Phys.* **26**, 3835 (1993).
- [14] J. M. Monti, R. D. Rivarola, and P. D. Fainstein, Distorted wave theories for dressed-ion-atom collisions with GSZ projectile potentials, *J. Phys. B: At., Mol. Phys.* **44**, 195206 (2011).
- [15] J. M. Monti, M. A. Quinto, and R. D. Rivarola, A complete CDW theory for the single ionization of multielectronic atoms by bare ion impact, *Atoms* **9**, 3 (2021).
- [16] D. Burch, H. Wieman, and W. B. Ingalls, Electron Loss in High-Energy Oxygen-Ion Collisions, *Phys. Rev. Lett.* **30**, 823 (1973).
- [17] W. E. Wilson and L. H. Toburen, Electron emission in  $\text{H}_2^+$ - $\text{H}_2$  collisions from 0.6 to 1.5 MeV, *Phys. Rev. A* **7**, 1535 (1973).
- [18] T. J. M. Zouros, P. Richard, K. L. Wong, H. I. Hidmi, J. M. Sanders, C. Liao, S. Grabbe, and C. P. Bhalla, Projectile charge-state dependence of zero-degree binary encounter electron production in 30 MeV  $\text{O}^{q+} + \text{O}_2$  collisions, *Phys. Rev. A* **49**, R3155 (1994).
- [19] T. J. M. Zouros, K. L. Wong, S. Grabbe, H. I. Hidmi, P. Richard, E. C. Montenegro, J. M. Sanders, C. Liao, S. Hagmann, and C. P. Bhalla,  $0^\circ$  binary encounter electron production in 30-MeV  $\text{O}^{q+} + \text{H}_2$ , He,  $\text{O}_2$ , Ne, and Ar collisions, *Phys. Rev. A* **53**, 2272 (1996).
- [20] T. J. M. Zouros, G. Toth, P. Richard, C. Liao, and S. Hagmann, Zero-degree binary encounter electron production in 30 MeV bare  $\text{O}^{8+}$  in collisions with  $\text{H}_2$ , He, Ne, Ar, Kr and Xe, *Nucl. Instrum. Methods Phys. Res. B* **107**, 87 (1996).
- [21] C. R. Vane, I. A. Sellin, M. Suter, G. D. Alton, S. B. Elston, P. M. Griffin, and R. S. Thoe, Z, Velocity, and Charge Dependence of Zero-Degree Electron “cusps” from Charge Transfer to Continuum States of Bare and Highly Ionized Projectiles, *Phys. Rev. Lett.* **40**, 1020 (1978).
- [22] M. Breinig, S. B. Elston, S. Huld, L. Liljeby, C. R. Vane, S. D. Berry, G. A. Glass, M. Schauer, I. A. Sellin, G. D. Alton, S. Datz, S. Overbury, R. Laubert, and M. Suter, Experiments concerning electron capture and loss to the continuum and convoy electron production by highly ionized projectiles in the 0.7–8.5-MeV/u range transversing the rare gases, polycrystalline solids, and axial channels in gold, *Phys. Rev. A* **25**, 3015 (1982).
- [23] D. H. Lee, P. Richard, T. J. M. Zouros, J. M. Sanders, J. L. Shinpaugh, and H. Hidmi, Binary encounter electrons observed at zero degrees in collisions of 1–2 MeV/amu  $\text{H}^+$ ,  $\text{C}^{6+}$ ,  $\text{N}^{7+}$ ,  $\text{O}^{8+}$  and  $\text{F}^{9+}$ , *Phys. Rev. A* **41**, 4816 (1990).
- [24] M. Rodbro and F. Andersen, Charge transfer to the continuum for 15 to 1500 keV  $\text{H}^+$  in He, Ne, Ar and  $\text{H}_2$  gases under single-collision conditions, *J. Phys. B: At., Mol. Phys.* **12**, 2883 (1979).
- [25] J. B. Crooks and M. E. Rudd, Angular and energy distribution of cross sections for electron production by 50–300-keV-proton impacts on  $\text{N}_2$ ,  $\text{O}_2$ , Ne, and Ar, *Phys. Rev. A* **3**, 1628 (1971).
- [26] W. Meckbach, I. B. Nemirovsky, and C. R. Garibotti, Resolution dependence and asymmetry of electron capture to the continuum spectra, *Phys. Rev. A* **24**, 1793 (1981).
- [27] L. Sarkadi, J. Bossler, R. Hippler, and H. O. Lutz, Electron Capture to Continuum States From Inner Shells, *Phys. Rev. Lett.* **53**, 1551 (1984).
- [28] A. E. Skutlartz, S. Hagmann, and H. Schmidt-Böcking, Correlated electron capture in the impact parameter and final projectile charge-state dependence of ECC cusp production in  $0.53 \text{ MeV } \text{u}^{-1} \text{F}^{8+} + \text{Ne}$ , *J. Phys. B: At., Mol. Phys.* **21**, 3609 (1988).
- [29] G. Bernardi, P. Fainstein, C. R. Garibotti, and S. Suarez, Projectile charge dependence of the ionisation spectra for  $\text{H}^+$  and  ${}^3\text{He}^{2+}$  ions on He and Ne atoms, *J. Phys. B: At., Mol. Phys.* **23**, L139 (1990).
- [30] T. J. Gay, M. W. Gealy, and M. E. Rudd, Projectile- and target-charge dependent effects in ionizing collisions of  $\text{H}^+$  and  ${}^3\text{He}^{2+}$  with He, Ne and Ar atoms, *J. Phys. B: At., Mol. Phys.* **23**, L823 (1990).
- [31] S. Suárez, C. Garibotti, W. Meckbach, and G. Bernardi, Experimental Evidence of the Asymmetry of the Soft Electron Peak in Ion-Atom Ionization, *Phys. Rev. Lett.* **70**, 418 (1993).
- [32] S. Biswas, D. Misra, J. M. Monti, C. A. Tachino, R. D. Rivarola, and L. C. Tribedi, Energy and angular distribution of electrons in ionization of He and Ne by 6-MeV/u bare carbon ions: Comparison with continuum-distorted-wave eikonal-initial-state calculations in prior and post forms, *Phys. Rev. A* **90**, 052714 (2014).
- [33] L. Sarkadi, J. Pálinkás, A. Kövér, D. Berényi, and T. Vajnai, Observation of Electron Capture into Continuum States of Neutral Atoms, *Phys. Rev. Lett.* **62**, 527 (1989).
- [34] T. Weber, K. Khayyat, R. Dörner, V. D. Rodríguez, V. Mergel, O. Jagutzki, L. Schmidt, K. A. Müller, F. Afaneh, A. Gonzalez, and H. Schmidt-Böcking, Abrupt Rise of the Longitudinal Recoil Ion Momentum Distribution for Ionizing Collisions, *Phys. Rev. Lett.* **86**, 224 (2001).
- [35] P.-M. Hillenbrand, S. Hagmann, D. H. Jakubassa-Amundsen, J. M. Monti, D. Banaś, K.-H. Blumenhagen, C. Brandau, W. Chen, P. D. Fainstein, E. De Filippo, A. Gumberidze, D. L. Guo, M. Lestinsky, Y. A. Litvinov, A. Müller, R. D. Rivarola, H. Rothard, S. Schippers, M. S. Schöffler, U. Spillmann *et al.*,

- Electron-capture-to-continuum cusp in  $U^{88+} + N_2$  collisions, *Phys. Rev. A* **91**, 022705 (2015).
- [36] P.-M. Hillenbrand, S. Hagmann, D. Atanasov, D. Banaš, K.-H. Blumenhagen, C. Brandau, W. Chen, E. De Filippo, A. Gumberidze, D. L. Guo, D. H. Jakubassa-Amundsen, O. Kovtun, C. Kozhuharov, M. Lestinsky, Y. A. Litvinov, A. Müller, R. A. Müller, H. Rothard, S. Schippers, M. S. Schöffler *et al.*, Radiative-electron-capture-to-continuum cusp in  $U^{88+} + N_2$  collisions and the high-energy endpoint of electron-nucleus bremsstrahlung, *Phys. Rev. A* **90**, 022707 (2014).
- [37] P.-M. Hillenbrand, S. Hagmann, M. E. Groshev, D. Banaš, E. P. Benis, C. Brandau, E. De Filippo, O. Forstner, J. Glorius, R. E. Grisenti, A. Gumberidze, D. L. Guo, B. Hai, M. O. Herdrich, M. Lestinsky, Y. A. Litvinov, E. V. Pagano, N. Petridis, M. S. Sanjari, D. Schury *et al.*, Radiative electron capture to the continuum in  $U^{89+} + N_2$  collisions: Experiment and theory, *Phys. Rev. A* **101**, 022708 (2020).
- [38] T. J. M. Zouros and D. H. Lee, Zero degree Auger electron spectroscopy of projectile ions, in *Accelerator-Based Atomic Physics: Techniques and Applications*, edited by S. M. Shafroth and J. C. Austin (AIP, Woodbury, NY, 1997), Chap. 13, pp. 426–479.
- [39] S. Harissopoulos, M. Andrianis, M. Axiotis, A. Lagoyannis, A. G. Karydas, Z. Kotsina, A. Laoutaris, G. Apostolopoulos, A. Theodorou, T. J. M. Zouros, I. Madesis, and E. P. Benis, The Tandem Accelerator Laboratory of NCSR Demokritos: Current status and perspectives, *Eur. Phys. J. Plus* **136**, 617 (2021).
- [40] I. Madesis, A. Dimitriou, A. Laoutaris, A. Lagoyannis, M. Axiotis, T. Mertzimekis, M. Andrianis, S. Harissopoulos, E. P. Benis, B. Sulik, I. Valastyán, and T. J. M. Zouros, Atomic physics with accelerators: Projectile electron spectroscopy (APAPES), *J. Phys.: Conf. Ser.* **583**, 012014 (2015).
- [41] I. Madesis, A. Laoutaris, T. J. M. Zouros, S. Nanos, and E. P. Benis, Projectile electron spectroscopy and new answers to old questions: Latest results at the new atomic physics beamline in Demokritos, Athens, in *State-of-the-Art Reviews on Energetic Ion-Atom and Ion-Molecule Collisions*, Interdisciplinary Research on Particle Collisions and Quantitative Spectroscopy Vol. 2, edited by D. Belkić, I. Bray, and A. Kadyrov (World Scientific, Singapore, 2019), Chap. 1, pp. 1–31.
- [42] T. J. M. Zouros and E. P. Benis, The hemispherical deflector analyser revisited. I. Motion in the ideal  $1/r$  potential, generalized entry conditions, Kepler orbits and spectrometer basic equation, *J. Electron Spectrosc. Relat. Phenom.* **125**, 221 (2002).
- [43] D. Belkić, A quantum theory of ionisation in fast collisions between ions and atomic systems, *J. Phys. B: At., Mol. Phys.* **11**, 3529 (1978).
- [44] I. M. Cheshire, Continuum distorted wave approximation; resonant charge transfer by fast protons in atomic hydrogen, *Proc. Phys. Soc.* **84**, 89 (1964).
- [45] D. Belkić, R. Gayet, and A. Salin, Electron capture in high-energy ion-atom collisions, *Phys. Rep.* **56**, 279 (1979).
- [46] P. D. Fainstein, V. H. Ponce, and R. D. Rivarola, A theoretical model for ionisation in ion-atom collisions. Application for the impact of multicharged projectiles on helium, *J. Phys. B: At., Mol. Phys.* **21**, 287 (1988).
- [47] J. M. Monti, O. A. Fojón, J. Hanssen, and R. D. Rivarola, Influence of the dynamic screening on single-electron ionization of multi-electron atoms, *J. Phys. B: At., Mol. Phys.* **43**, 205203 (2010).
- [48] E. Clementi and C. Roetti, Roothaan-Hartree-Fock atomic wavefunctions: Basis functions and their coefficients for ground and certain excited states of neutral and ionized atoms,  $Z \leq 54$ , *At. Data Nucl. Data Tables* **14**, 177 (1974).
- [49] J. M. Monti, O. A. Fojón, J. Hanssen, and R. D. Rivarola, Single electron ionization of multishell atoms: Dynamic screening and post-prior discrepancies in the CDW-EIS model, *J. Phys. B: At., Mol. Phys.* **46**, 145201 (2013).
- [50] P. P. Szydlik and A. E. Green, Independent-particle-model potentials for ions and neutral atoms with  $Z \leq 18$ , *Phys. Rev. A* **9**, 1885 (1974).
- [51] D. S. F. Crothers and J. F. McCann, Ionisation of atoms by ion impact, *J. Phys. B: At., Mol. Phys.* **16**, 3229 (1983).
- [52] L. Gulyás, P. D. Fainstein, and A. Salin, CDW-EIS theory of ionization by ion impact with Hartree-Fock description of the target, *J. Phys. B: At., Mol. Phys.* **28**, 245 (1995).
- [53] J. M. Monti, O. A. Fojón, J. Hanssen, and R. D. Rivarola, Ionization of helium targets by proton impact: A four-body distorted wave-eikonal initial state model and electron dynamic correlation, *J. Phys. B: At., Mol. Phys.* **42**, 195201 (2009).
- [54] L. Gulyás and T. Kirchner, Ionization of Ar by energetic proton impact, *Phys. Rev. A* **70**, 022704 (2004).
- [55] V. H. Ponce, Velocity parameters of atomic wavefunctions, *At. Data Nucl. Data Tables* **19**, 63 (1977).